

# Pigmento: Pigment-Based Image Analysis and Editing

Jianchao Tan\*  
George Mason University

Stephen DiVerdi†  
Adobe Research

Jingwan Lu‡  
Adobe Research

Yotam Gingold§  
George Mason University

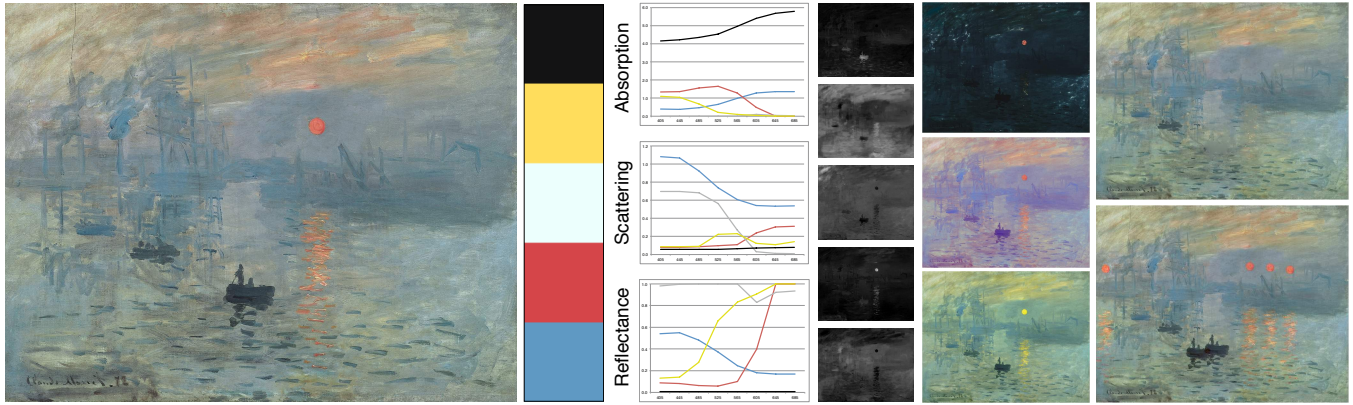


**Figure 1:** Analysis and editing of Monet’s “Impression, soleil levant.” From left to right, input image, extracted palette in RGB, multispectral coefficient curves for palette pigments, mixing weights, recoloring, and cut-copy-paste.

## Abstract

The colorful appearance of a physical painting is determined by the distribution of paint pigments across the canvas, which we model as a per-pixel mixture of a small number of pigments with multispectral absorption and scattering coefficients. We present an algorithm to efficiently recover this structure from an RGB image, yielding a plausible set of pigments and a low RGB reconstruction error. We show that under certain circumstances we are able to recover pigments that are close to ground truth, while in all cases our results are always plausible. Using our decomposition, we repose standard digital image editing operations as operations in pigment space rather than RGB, with interestingly novel results. We demonstrate tonal adjustments, selection masking, cut-copy-paste, recoloring, palette summarization, and edge enhancement.

**Keywords:** painting, color, RGB, non-photorealistic editing, NPR, kubelka-munk, pigment, paint, mixing, layering, image, editing

**Concepts:** •Computing methodologies → Image manipulation; Image processing;

## 1 Introduction

Stated generally, a “painting” in the physical world is a two-dimensional arrangement of material. This material may be oil or watercolor paint, or it may be ink from a pen or marker, or charcoal or pastel. These pigments achieve a colorful appearance by virtue of how they absorb and reflect light and their thickness. Kubelka and Munk [Kubelka and Munk 1931; Kubelka 1948] described a model for the layering of physical materials, and Duncan [Duncan 1940] extended it to include homogeneous mixing. In this model, the appearance of a material (reflectance and transmission of light) is defined by how much it scatters and absorbs each wavelength of light and its overall thickness. These models are widely used to

model the appearance of paint, plastic, paper, and textiles; they have been used previously in the computer graphics literature [Curtis et al. 1997; Baxter et al. 2004; Lu et al. 2014; Tan et al. 2015].

When painting, artists choose or create a relatively small set of pigments to be used throughout the painting. We call this set the *primary pigment palette*. We assume that all observed colors in the painting are created by mixing or layering pigments from the palette.

When we view a painting, either directly with our eyes or indirectly after digitizing it into a three-channel RGB image, we observe only the overall reflectance and not the underlying material parameters. In RGB-space, the underlying pigments which combine to form the appearance of a pixel are not accessible for editing. One color in the palette cannot be easily changed or replaced. Translucent objects, common in paintings due to the mixing of wet paint, cannot be easily extracted or inserted.

We propose an approach to decompose a painting into its constituent pigments in two stages. First, we compute a small set of pigments in terms of their Kubelka-Munk (KM) scattering and absorption parameters. Second, we compute per-pixel mixing proportions for the pigments that reconstruct the original painting. We show that this decomposition has many desirable properties. Particularly for images of paintings, it is able to achieve lower error reconstructions with smaller palettes than previous work. Furthermore, the decomposition enables image editing applications to be posed in pigment space rather than RGB space, which can make them more effective or more expressive. We demonstrate tonal adjustments by editing pigment properties; recoloring; selection masking; copy-paste; palette summarization; and edge enhancement.

Thematically, this work is similar to Lillicon [Bernstein and Li 2015] and Project Naptha [Kwok and Webster 2016], which both present ways to interpret structure in unstructured documents to enable high level edits based on the interpreted structure. In Lillicon’s case, the structure is an alternate vector representation of the artwork, while in Project Naptha, the structure is styled text within the image. Our contribution is to apply this strategy to flat, unstructured RGB images of paintings, which are created via deep structure (physical pigments and brush strokes). Our analysis allows us to interpret the

\*e-mail: tanjianchaoustc@gmail.com

†e-mail: stephen.diverdi@gmail.com

‡e-mail: jingwan.lu.cynthia@gmail.com

§e-mail: ygingold@gmu.edu

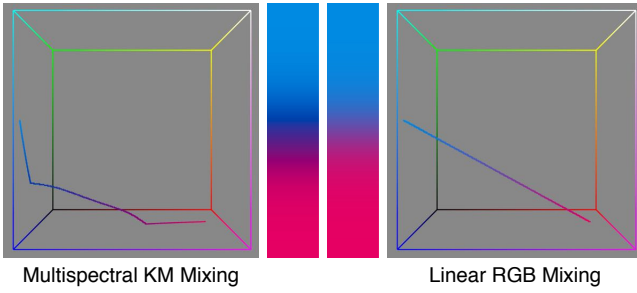


**Figure 2:** Comparing mixing models. The left gradient interpolates between cyan and magenta pigments using the KM equation, while the right gradient interpolates the same colors in linear RGB. The resulting colors are plotted as curves in the RGB color cube. The shape of the left curve is due to the non-linear nature of KM rendering, clipping, and gamma correction.

deep structure of the painting from the RGB image, which enables editing operations based on that structure.

## 2 Related Work

Our work directly follows from the efforts of Tan et al. [2016] and Lin et al. [2017], both of which propose different mechanisms for decomposing an arbitrary image into a small set of partially transparent RGB layers that reconstructs the image. This decomposition allows editing of the image in a potentially more intuitive way, effectively segmenting the image by color and spatial coherence. Similarly, Chang et al. [2015] extract a small palette of colors from an image, and implicitly model each pixel as a mixture of those palette colors to enable recoloring. We extend these results specifically for images of paintings by estimating multispectral properties of real pigments, instead of RGB colors.

Algorithmically, our work is most similar to that of Kauvar et al. [2015], which optimizes a set of multispectral illuminants and mixing weights to reproduce an image. The complexity of the Kubelka-Munk equations makes our problem much harder.

While the Kubelka-Munk (KM) equations [Kubelka and Munk 1931] can be used to reproduce the color of a layer of pigment, they are difficult to acquire [Okumura 2005], so researchers have pursued a simplified model. Curtis et al. [1997] use a three wavelength model they compute from samples of paint over white and black backgrounds. In our multispectral scenario given RGB data and a fixed background, direct extraction is impossible. The IMPaSto system [Baxter et al. 2004] uses a low dimensional approximation of measured pigments to enable realtime rendering. In contrast, we focus on the problem of decomposing existing artwork. Xu et al. [2007] use a neural network to learn to predict RGB colors from a large number of synthetic examples. RealPigment [Lu et al. 2014] estimates composited RGB colors from exemplar photos of artist color mixing charts. In our scenario, we are given the RGB colors and estimate the multispectral scattering and absorption parameters.

There is extensive work on multispectral acquisition systems using custom hardware [Boldrini et al. 2012]. Berns et al. [2005a] use a standard digital camera with a filter array. Parmar et al. [2012] use a bank of LEDs to capture the scene under different illumination spectra. Park et al. [Park et al. 2007] optimize a set of exposures and LED illuminants to achieve video rates. Multispectral images have many useful applications. Ibrahim et al. [2016] demonstrate intrinsic image reconstruction and material identification. Berns et al. [Berns et al. 2005b] compare a multispectral imager to a point

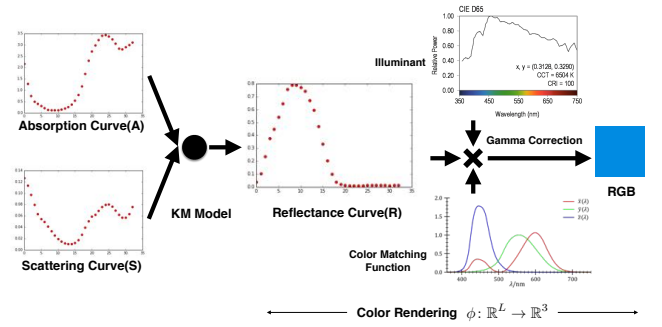


**Figure 3:** Rendering from multispectral KM coefficients (absorption and scattering) to sRGB color, for cyan pigment, totally 33 wavelength range from 380nm to 700nm (every 10nm). It is rendered on pure white substrate with pigment thickness equal to 1, under D65 illuminant.

spectrophotometer for measurements of paintings.

Multispectral imaging is a non-invasive way to preserve paintings and analyze their construction. Berns et al. [2002] estimate the full reflectance spectrum of a painting using a reduced dimension parameterization made from spectra of known KM pigments. Zhao et al. [2005] achieve better reconstructions by fitting mixtures of known pigments to estimated multispectral reflectances. Pelagotti et al. [2008] and Cosentino [2014] both use multispectral images as feature maps to identify single layers of known pigments. Most similar to our work, Zhao et al. [2008] use multispectral measurements of Van Gogh’s “Starry Night” to estimate one parameter masstone KM mixing weights for known pigments to reconstruct the painting. All of these works require custom acquisition hardware, whereas we focus on standard RGB images only.

## 3 Theory

The intuition behind this work comes from how pigments mix in real versus digital media. Digital RGB color mixing is a linear operation: all mixtures of two RGB colors lie on the straight line between them. Mixing two physical pigments with the same apparent RGB colors, however, produces a curve of colors when rendering to RGB (Fig. 2). Similarly, when an opaque RGB color is gradually thinned to reveal the background, the result is a straight line in RGB-space. When a real physical pigment is thinned, the result is again a curve. The shape of this curve is a function of the multispectral Kubelka-Munk coefficients of the pigments being interpolated. Our intuition is that those multispectral coefficients can be deduced by the observed shape of a mixing or thinning curve in RGB.

### 3.1 Kubelka-Munk Equations

The Kubelka-Munk equations (KM) are a physical model that computes the per-wavelength reflectance value of a layer of homogeneous pigment of a thickness  $atop$  a substrate:

$$R = \frac{1 - r(a - b \cdot \coth(bSt))}{a - r + b \cdot \coth(bSt)} \quad (1)$$

$$a = 1 + \frac{A}{S}, \quad b = \sqrt{a^2 - 1}$$

where  $t$  is the thickness of the layer,  $A$  and  $S$  are the pigment’s absorption and scattering per unit thickness,  $r$  is the substrate reflectance, and  $R$  is the final reflectance of the pigment layer.  $A$ ,  $S$ ,  $r$ , and  $R$  are all per-wavelength, while the thickness  $t$  is constant for

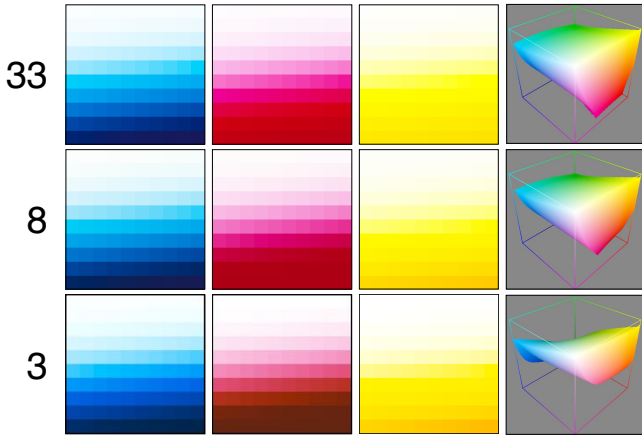


**Figure 4:** Visualizing rendering with different numbers of wavelengths. The original cyan, magenta, and yellow pigment coefficients, sampled at 33 wavelengths between 380nm and 700nm, are downsampled to 8 and 3 wavelengths and rendered with varying thickness. The RGB gamuts achieved by mixing them are plotted. The 8 wavelength gamut appears similar to the 33 wavelength gamut, but the 3-wavelength gamut is clearly distorted.

all wavelengths. For convenience, we use  $K = [A, S]$  to represent all the KM coefficients with a single variable. We denote Equation 1 as  $km(K, r, t)$ .

Mixtures of pigments are modeled as linear interpolation of the KM coefficients:

$$K = \frac{\sum w_i K_i}{\sum w_i} \quad (2)$$

To render a KM pigment to RGB requires knowing the pigment’s KM coefficients, the substrate reflectance, the layer thickness, the illuminant spectrum, and the color matching functions which map from a reflectance spectrum to a tristimulus value, which can then be converted to RGB and gamma corrected to sRGB. Figure 3 shows the pipeline for a single pigment. We use the D65 standard illuminant and CIE color matching functions [Ohta and Robertson 2006].

For a pixel in the image,  $R = km(K, r, t)$  yields a reflectance spectrum defined at each of the  $L$  wavelengths. We denote the spectrum rendering pipeline in Figure 3 as a function  $\phi: \mathbb{R}^L \rightarrow \mathbb{R}^3$ , so  $I_p = \phi(R_p)$  where  $I_p$  is the sRGB color for pixel  $p$ . Thus to render an image we have:

$$I = \phi(km(K, r, t)) \quad (3)$$

In contrast to RGB color compositing, this model is highly non-linear and is responsible for much of the “organic” feel of traditional media paints as compared to digital paintings (Fig. 2).

It is important to consider the required number of wavelengths to simulate. Too many wavelengths will be difficult to optimize, whereas too few may not be able to accurately reconstruct the image appearance. We experimented with mixtures of cyan, magenta, and yellow pigments from 33 wavelengths to 3. We found that below 8 wavelengths, the color reproduction loses fidelity (Fig. 4). We can also see that the size of the RGB gamut that can be reconstructed is artificially restricted at 3 wavelengths versus 8. This is in agreement with prior work such as RealPigment [Lu et al. 2014] and IMPaSTo [Baxter et al. 2004].

## 3.2 Problem Formation

A painter creates a palette from a set of e.g. tubes of paint, which we call the *primary pigments*. Every color in the painting is a mixture of these primary pigments. Therefore, mixtures of the primary pigments’ KM coefficients are sufficient to reproduce the RGB color of every pixel in the painting. Our method estimates the coefficients of a small set of primary pigments to minimize the RGB reconstruction error.

For  $L$  wavelengths, each primary pigment  $K_m$  is a vector of  $2L$  coefficients. We can represent the set of  $M$  primary pigments as an  $M \times 2L$  matrix  $H = [K_1, K_2, \dots, K_M]^T$ . Every pixel in the painting can be represented as a convex combination of these primary pigments,  $w_i \cdot H$ , where  $w_i$  is the  $1 \times M$  vector of mixing weights ( $0 \leq w_i \leq 1$ ). We can express all  $N$  pixels in the image as the matrix product  $WH$ , where the  $w_i$  form the rows of the  $N \times M$  matrix  $W$ . Eq. 3 becomes:

$$I = \phi(km(WH, r, t)) \quad (4)$$

where  $I$  is the  $N \times 3$  matrix of our painting’s per-pixel RGB colors.

To simplify the problem, we assume the canvas is pure white ( $r = 1$ ) and we assume that the entire canvas is uniformly covered with paint ( $t = 1$ ). Thus, our equation becomes:

$$I = \phi(km(WH)) \quad (5)$$

We can use Eq. 5 to pose an optimization problem:

$$\begin{aligned} E_{data} &= \|I - \phi(km(WH))\|^2 \\ E_{sum} &= \|W \mathbf{1}_{M \times 1} - \mathbf{1}_{N \times 1}\|^2 \\ W^*, H^* &= \argmin\{E_{data} + w_{sum} E_{sum}\} \end{aligned} \quad (6)$$

where  $\mathbf{1}_{M \times 1}$  and  $\mathbf{1}_{N \times 1}$  are column vectors of ones, and subject to the constraints  $0 \leq W \leq 1$  and  $H > 0$ .  $E_{sum}$  forces our per-pixel weights to sum to one, since each pixel’s coefficients are a convex combination of the primary pigments. As an alternative to  $E_{sum}$ , one could use  $W = \text{softmax}(W')$  in  $E_{data}$ . This would allow unconstrained variation of  $W'$  while maintaining that the weights (rows) of  $W$  sum to one. However, in our experiments we found that  $E_{sum}$  has better convergence properties.

## 3.3 Solution Space

In Eq. 6,  $W$  and  $H$  are both unknown, so we have  $NM + 2LM$  unknown variables and  $3N + N$  known equations, which makes our problem under-constrained for  $M > 3$ . We can use regularization to make the problem over-constrained. While this results in a solution, there are infinitely many solutions to the problem as originally stated for any particular image. This is for two reasons.

First,  $\phi(\cdot)$  projects from  $L$ -dimensional reflectance spectra to 3-dimensional *tristimulus* values. For any given tristimulus value there are infinitely many possible spectra that could produce it. This is analogous to seeing only the 2D projection or “shadow” of a 3D curve. No matter how many high dimensional samples we obtain,  $\phi$  projects them all in parallel.

Second, if there exists  $G$  s.t.  $WH = WGG^{-1}H$ , for  $0 \leq WG \leq 1$ , and  $G^{-1}H > 0$ , then  $W' = WG$  and  $H' = G^{-1}H$  is another solution that generates the same RGB result. In a simple geometric sense,  $G$  could be a rotation or a scale. So long as the set of observed pigment parameters all lie within the polytope whose vertices are the rows of  $H$ , then e.g. rotations and scales that maintain that property will also produce solutions. If the colors are near the edges of the



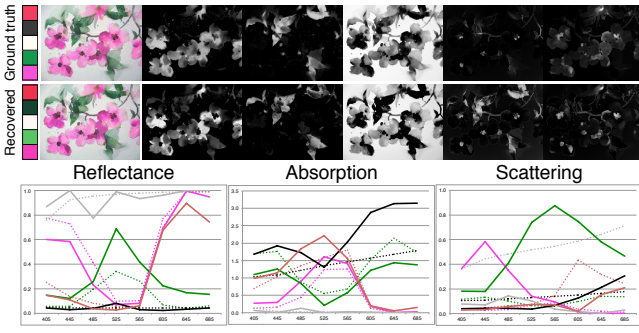


**Figure 5:** Recovering ground truth. Our reconstruction is low RGB error and the palette and mixing weight maps are similar upon inspection. The graphs of spectral curves show reflectances are recovered well, but absorption and scattering less so. Numeric results are in Table 2. Ground truth curves are dashed, recovered are solid, and colors correspond to palette colors. Note: ground truth black’s coefficients have been scaled by 0.2, effectively thinning the paint, to achieve a similar range.

gamut, or the pigment parameters are near the edges of the KM space (i.e. have small values in the KM coefficients), then there will be very little “wiggle room” for the pigments to move. Conversely, if the set of observed pigment parameters are compact (i.e. no KM coefficients near zero), then many different gamuts may be possible.

## 4 Method

Our naively posed optimization problem (Eq. 6) is too slow to run on an entire, reasonably-sized image at once. To improve performance, we decompose our task into two subproblems: estimating primary pigments and estimating per-pixel mixing weights.

### 4.1 Estimating Primary Pigments

The first step in our pipeline is to estimate a set of primary pigment coefficients  $H$  that can reconstruct the painting. Even for small input images of 0.25 megapixels, doing this estimation over every pixel in the image would be computationally very expensive. We observe that it is not necessary to consider every pixel, since many pixels contain redundant information. Therefore, we optimize over a small subset of representative pixels, carefully chosen to well-represent the image’s color properties.

To find a small subset of representative pixels, we find the 3D convex hull of the set of RGB colors in the image using the QHull algorithm [Barber et al. 1996]. For the images we tested, this usually results in a few hundred unique colors. These pixels are particularly well suited to the task of estimating the primary pigments because they span the full gamut of the painting’s colors. They are guaranteed to include the most extreme combinations of pigments. Conversely, pixels in the interior of the convex hull are less distinct, resulting in less vibrant primary pigments.

Even with this smaller set of pixels, the optimization problem as posed in Eq. 6 is very similar to non-negative matrix factorization—which is non-convex—with the added non-linearities of the KM equation and gamma correction. Therefore, we use the Alternating Nonlinear Least Squares (ANLS) method for our optimization.

In the first step, we fix the set of primary pigment coefficients  $H$  and solve for the mixing weights  $W$ :

$$W^* = \operatorname{argmin}\{E_{data} + w_{sum}E_{sum}\} \quad (7)$$

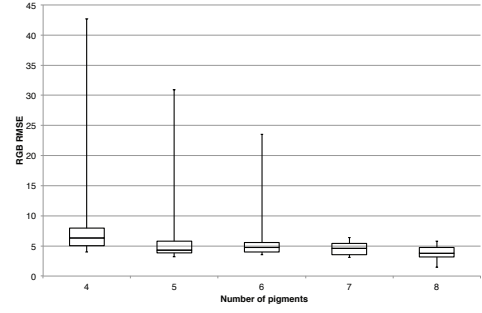


**Figure 6:** We plot distribution of 12 examples’ image reconstruction RGB RMSE on different palette size. Generally, RMSE will decrease when palette size increase, and RMSE distribution deviation will decrease when palette size increase.

with the constraint  $0 \leq W \leq 1$ , and  $w_{sum} = 10.0$ .

In the second step, we fix  $W$  and solve for  $H$ . When estimating the primary pigments, we add an additional regularization term to avoid creating physically implausible pigment coefficients. Specifically, KM pigment coefficients  $A$  and  $S$  should vary smoothly across wavelengths [Lu et al. 2014], and the ratio  $\frac{A}{S}$  (which determines the pigment’s masstone) should also vary smoothly across wavelengths. We encode these smoothness observations as:

$$E_{smooth} = \frac{N}{M(L-1)} \sum_{i=1}^M \sum_{j=1}^{L-1} \left( \lambda_A (A_{i,j} - A_{i,j+1})^2 + \lambda_S (S_{i,j} - S_{i,j+1})^2 + \lambda_{ratio} \left( \frac{A_{i,j}}{S_{i,j}} - \frac{A_{i,j+1}}{S_{i,j+1}} \right)^2 \right) \quad (8)$$

over all  $M$  primary pigments and  $L$  wavelengths, where  $\lambda_A = \lambda_S = 1$  and  $\lambda_{ratio} = 0.001$  control the relative influence of the terms. Putting it all together, our optimization for the second step is:

$$H^* = \operatorname{argmin}\{E_{data} + w_{smooth}E_{smooth}\} \quad (9)$$

with the constraint  $H > 0$  and  $w_{smooth} = 0.001$ .

**Initialization** As with any non-convex optimization problem, initialization is a key factor in how quickly the solution converges and whether a local minimum is found. In our case, the solution is not unique, so there are many potential minima to converge upon. Therefore, initialization is very important for finding a good solution.

One option is to initialize randomly, which produces somewhat unpredictable results, though we do find that plausible solutions (where the colors of the primary pigments roughly match a painter’s expectations) are often well-represented. In the absence of other information, we can present the user with the results of e.g. ten random initializations to choose their preferred solution.

An alternative is to take advantage of a prior, such as a natural distribution of real pigments in KM space. We use a set of 26 measured acrylic paints from Okumura [2005]. When the prior is similar to the pigments used in the painting, reconstruction often finds the approximately correct KM coefficients. When the prior is of a different media than the painting (e.g. using an acrylic prior with a watercolor painting), then while the result will have low reconstruction error and look plausible, the mixing properties of the pigments may not be correct (e.g. a watercolor painting may have more opaque pigments in the reconstruction than in reality). When

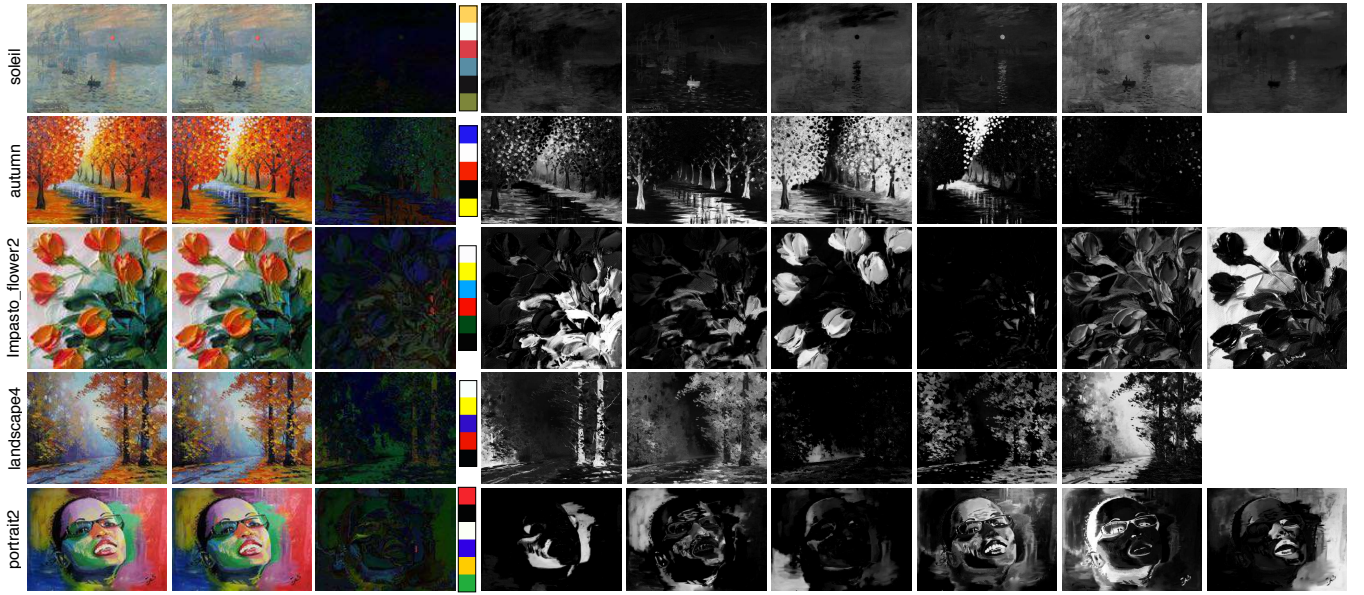


**Figure 7:** Our results for multiple images, one per row. From left to right the columns are the original image, the reconstruction, the error (10x), the extracted palette, and the mixing weight maps. While our pigments are multispectral, we only show the RGB colors when rendered on a white canvas with unit thickness.

multiple such priors are available, a user could select the correct prior to use for a given painting. In our experiments, we rely on the dictionary of Okumura’s 26 acrylic pigments. To boost the size of the dictionary, we also include every pair of pigments mixed 50%, for a total of 351 entries.

To initialize  $H$  with  $M$  pigments using our prior, we start from the convex hull of the RGB colors in the image. We simplify the convex hull to  $M$  vertices as in Tan et al. [Tan et al. 2016]. We then match these  $M$  RGB colors to the closest matching (Euclidean distance) RGB colors in the dictionary and use the corresponding KM coefficients. The RGB color of a dictionary pigment is obtained by rendering with the same pipeline as Eq. 3 (with thickness  $t = 1$  and substrate  $r = 1$ ). If two convex hull colors match to the same dictionary color, the closer match is used and the other convex hull vertex matches to its second closest dictionary color.

## 4.2 Estimating Mixing Weights

The second step of our pipeline uses the estimated set of primary pigments to compute per-pixel mixing weights for the entire image. We use observations about the nature of painting construction to add additional regularization terms, improving convergence and making the results more useful for editing applications.

First, we add a term for per-pixel weights sparsity, which encourages each pixel’s  $M$  pigment weights to be close to 0 or 1:

$$E_{\text{sparse}} = -\frac{1}{M} \|\mathbf{1}_{N \times M} - W\|^2 \quad (10)$$

where  $\mathbf{1}_{N \times M}$  is matrix of ones. This term has the effect of maximizing color separation throughout the painting, so that each pigment influences as small a portion of the image as possible. This is desirable because it results in more localized pigment editing operations.

Second, we add a term for spatial smoothness of the weights:

$$E_{\text{spatial}} = \frac{1}{M} \|SW\|^2 \quad (11)$$

where  $S$  is a Laplacian or a bilateral smoothing matrix. We use a bilateral operator [Barron and Poole 2016] in order to preserve edges that appear between brush strokes of different colors of paint. In our experiments, the Laplacian operator blurred edges and caused pigments to incorrectly bleed into image regions.

With these additional terms, our optimization to reconstruct mixing weights becomes:

$$W^* = \operatorname{argmin}\{E_{\text{data}} + w_{\text{sum}}E_{\text{sum}} + w_{\text{sparse}}E_{\text{sparse}} + w_{\text{spatial}}E_{\text{spatial}}\} \quad (12)$$

where  $w_{\text{sum}} = 10$ ,  $w_{\text{sparse}} = 0.1$ , and  $w_{\text{spatial}} = 1$  subject to  $0 \leq W \leq 1$ ,

This optimization is still very large and difficult to solve directly. Instead, we solve it recursively. We downsample the image by factors of two until the short edge is less than 80 pixels. We solve the optimization on the smallest image, initializing each pixel’s mixing weights to  $1/M$ . We upsample each solution (mixing weights) as the initialization for the next larger optimization. We repeat this procedure until the original image is solved.

## 5 Results

To demonstrate our results, we conduct a series of experiments on synthetic and real images, comparing amongst different conditions and with previous work. All tests were run on a single core of either a 2.53 GHz Intel Xeon E5630 or a 2.50 GHz Intel Core i7-4870HQ, implemented in Python using the L-BFGS-B [Zhu et al. 1997] solver. Runtime information is presented in Table 1, which shows that we are generally faster than previous work [Tan et al. 2016]. Once the primary pigments and mixing weights are estimated, all of our editing applications occur in realtime.

**Synthetic Data** We use synthetic images to evaluate our pipeline’s recovery performance against ground truth. We use five weight maps from a color-based decomposition of a painting and measured

**Table 1:** Performance data for Fig. 7 and 8. Our pipeline extracts  $M$  primary pigments in a few seconds and mixing weights maps in less than 10 minutes for a normal size image, with low RGB image reconstruction error.

Image	Size	M	CPU	Primary (sec)	Weights (sec)	RGB RMSE
soleil	600×467	6	i7	35	155	1.9
autumn	600×458	5	xeon	16	255	6.0
four_colors_2	600×598	4	i7	9	211	5.2
Impasto_flower2	595×600	6	xeon	44	615	5.1
landscape4	600×479	5	xeon	26	256	4.7
portrait2	600×441	6	xeon	29	243	4.4
tree	600×492	4	i7	14	151	4.0

KM coefficients of real acrylic paints [Okumura 2005]. We create five synthetic paintings using random pigments and render them to sRGB with Eq. 3. To make our initialization fair, we use a hold-one-out methodology for the pigment dictionary: we remove the five pigments used to construct a synthetic image from the set of candidate pigments for initialization, leaving a dictionary of 21 (plus mixed pigments, so 231 in total). Fig. 5 shows an example of one of the synthetic images and its recovery, and all the reconstruction errors are presented in Table 2.

The results of this experiment are that the pigment coefficients  $A$  and  $S$  have relatively high error, where for our measured pigments,  $A \in [0, 10]$  and  $S \in [0, 1]$ . Our reflectance spectra have lower error, because there are many values of  $A$  and  $S$  that can create the same appearance. Since the pigments are different from ground truth, the recovered weight maps  $W$  are too, but the RGB reconstruction error is quite small, generally below the noticeable threshold. We can test the weight map recovery step in isolation by using the ground truth pigments to estimate  $W^*$  which has a smaller error but still significant, but the final RGB\* error stays low. This experiment confirms that there are many solutions to our reconstruction problem, but that we are able to reproduce plausible values.

**Table 2:** Reconstruction errors for synthetic data experiments (Fig. 5) with constant weight maps and different pigments. Each reported number is RMSE, for pigment absorption  $A$  and scattering  $S$  coefficients, and reflectance  $R$ . From those pigments, weight map  $W$  and RGB image are recovered. To test weight map recovery in isolation,  $W^*$  and RGB\* use the ground truth pigments.

Exp	A	S	R	W	W*	RGB	RGB*
1	6.1	1.2	0.3	29.0	15.2	4.8	5.8
2	1.4	0.9	0.3	19.8	11.8	6.8	4.3
3	4.5	0.5	0.7	63.0	21.4	6.7	5.9
4	7.1	1.2	0.6	42.3	14.1	8.5	6.0
5	1.0	0.7	0.3	16.6	10.4	5.8	5.2
Mean	4.0	0.9	0.4	34.1	14.6	6.5	5.5
Std	2.7	0.3	0.2	19.0	4.2	1.4	0.7

**Influence of Palette Size** Since the number of primary pigments is not automatically determined by our algorithm, we test on a set of images over a wide range of palette sizes to see how the reconstruction error behaves (Fig. 6). Unsurprisingly, as the number of pigments increases, aggregate reconstruction error goes down. Interestingly, each image seems to have a number of pigments after which the RMSE stops decreasing which intuitively would be the natural number of pigments in the painting. For paintings with very large numbers of pigments, it is unlikely that this property would

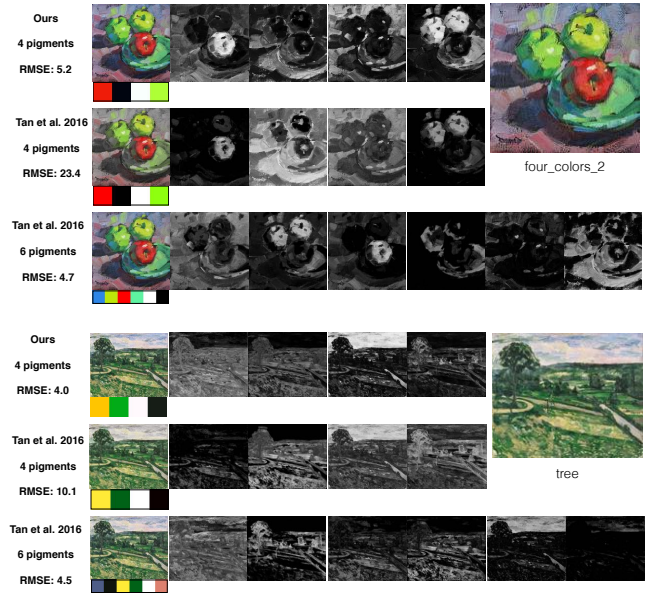


**Figure 8:** Comparison with Tan2016. When matching number of colors, Tan2016 has higher reconstruction error. To match our reconstruction error, Tan2016 needs to use more colors.

hold, as eventually a large set of primary pigments would be over-complete and no additional information could be gained. However, most painters use relatively small palettes in general.

**Real Images** We show our pipeline running on real images in Figures 7 and 8, with extracted primary pigments and weight maps and reconstructed RGB images. Reconstruction error is reported in Table 1. We tried from 4 to 6 pigments for every example, but only show the result with the smallest palette that gives good reconstruction. Painting four\_colors\_2 is known to have been created with only four paints: titanium white, cadmium yellow lemon, cadmium red, and ultramarine blue. Our extracted palette’s RGB colors are very similar, though the yellow is a bit greenish and the blue is dark.

**Comparison to Linear Model** Our algorithm uses multispectral pigments with the nonlinear KM model, in contrast to previous work [Tan et al. 2016] which solves a similar problem using linear RGB instead. Intuitively, we would expect that our model would be able to reconstruct paintings at lower error with fewer parameters, and the experiment we show in Fig. 8 confirms that. For two paintings, we show that we can reconstruct the images with low error for four pigments, whereas Tan2016 has much higher error for the same number of colors. In order to achieve a similar RGB reconstruction error, Tan2016 must increase to six colors in each case.

**Influence of Wavelengths** Our pipeline recovers 8 wavelength pigment absorption and scattering coefficients, because of the experiment in Figure 4 that shows a limited RGB gamut for 3 wavelength rendering. For completeness, we compare with 3 wavelength recovery in Figure 9. As 3 wavelength recovery is not multispectral anymore, we slightly amend our model equation, Eq. 3: we change the illuminant from D65 to pure white ( $\mathbf{1}_{3 \times 1}$ ), and we set the color matching function to be the identity matrix ( $\mathbf{I}_{3 \times 3}$ ). This has the effect of directly mapping the  $A$  and  $S$  coefficients to the RGB color channels, as done by Curtis et al. [1997].

We find that 3 wavelength recovery has larger RGB reconstruction



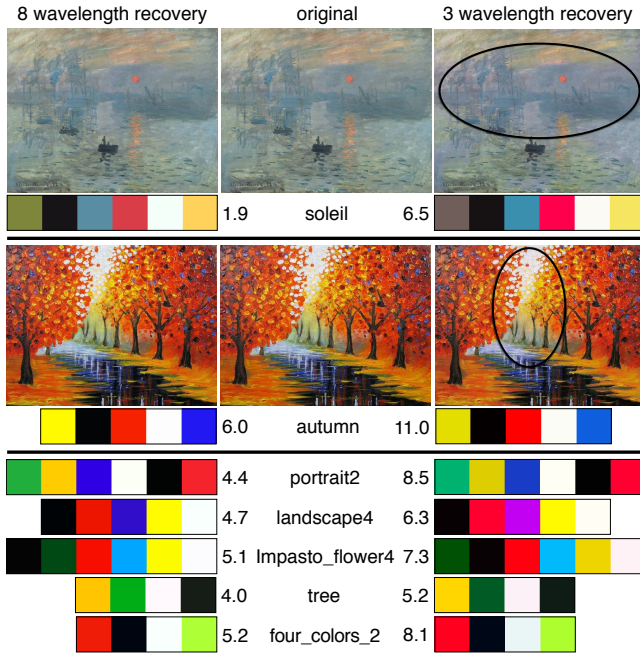


**Figure 9:** Comparison of 3 and 8 wavelength recovery, with RGB RMSE. We find 3 wavelength reconstruction error is higher for all examples. Soleil and autumn example show color distortion.

RMSE for the same size palettes in all of our experiments, though many of the achieved errors are still low enough to be generally unnoticeable. For some images, such as the two pictured in Fig. 9, there is obvious color distortion. We believe this is due to the restricted gamut of the 3 wavelength pigment model, which has a significant (visible) impact only on paintings that include colors in those extreme portions of the gamut, notably certain greens and reds. For paintings with colors entirely within the 3 wavelength gamut, the differences will be negligible.

We also compare 3 wavelength recovery with linear RGB [Tan et al. 2016] on example images tree and four.colors.2 in Fig. 8 and 9. The 3 wavelength KM recovery still produces better RGB reconstruction error for the same number of colors than the linear model.

## 6 Applications

Once we have analyzed a painting to extract its primary pigments (inset for most figures) and mixing weight maps, we can re-pose a number of image editing operations in pigment space to enable interesting paint-aware applications.

### 6.1 Masking

Selection masking in images of paintings can be improved by optimizing on pigment weights instead of RGB colors. Semantic image boundaries are likely to correspond with changes in paint, whereas RGB edges may be less obvious, when different paint mixtures are used to paint distinct objects. Also, paint thickness can create lighting variations across the surface of the painting that can confuse RGB boundary analysis. We demonstrate a standard GrabCut [Rother et al. 2004] implementation on two paintings on pigment maps vs. RGB values in Figure 10, which clearly shows improved localization of painted objects in the black rectangular regions. GrabCut was performed on the red pigment for the top painting, and on the black pigment for the bottom painting. No background and foreground

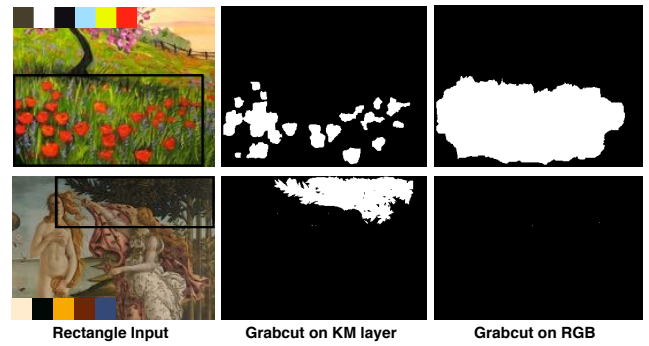


**Figure 10:** GrabCut on selected KM pigment mixing weights (top: red, bottom: black) outperforms GrabCut on the RGB image.

scribbles are provided to the GrabCut algorithm.

### 6.2 Adjustments

The pigment mixing maps provide a novel parameterization for image edits that may be difficult in RGB, by adjusting the relative values of the mixing weights, or adjusting the coefficients of the extracted pigments. First, we can vary the weight of any of the extracted pigments by scaling its map up or down and optionally re-normalizing the per-pixel weight sum to one. For a painting that has e.g. yellow pigment, this change corresponds to varying the amount of yellow in the image, in a way that would be difficult to reproduce using the features of a digital image manipulation program (Fig. 11).

Similarly, most extracted palettes include some white and black pigments for creating tints and shades. Adjusting the relative weights of these pigments is akin to adjusting the brightness and contrast of an image, but again with different results. For example, in Fig. 12a, the result of increasing the black weight is more like emphasizing shadows and detail, instead of just darkening, while the result of increasing the white weight is desaturation of the colors.

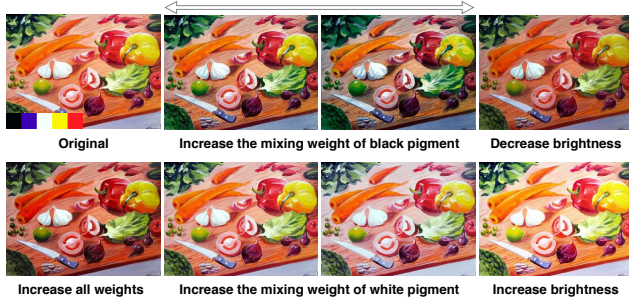
The KM coefficients of the pigments can also be relatively adjusted for interesting effects. Fig. 12b shows scaling the per-wavelength scattering coefficients of the green pigment, while keeping absorptions constant. Increasing scattering means that more light will be reflected back, so in some sense this is similar to brightening the green and making it more opaque, while decreasing scattering creates a darker green that absorbs more than it scatters, so perhaps more like a stained glass. Changing the scattering coefficients produces different hues of green compared to manipulating the pigment mixing weight (rightmost image in Fig. 12b).

### 6.3 Recoloring

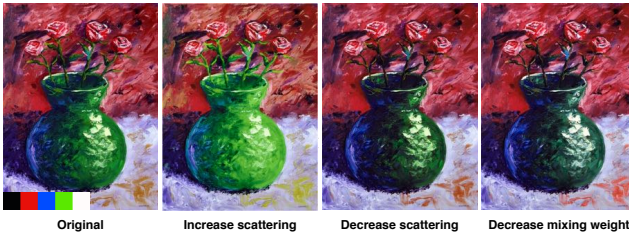
Previous work focused on recoloring images by changing the extracted palette colors. Tan et al. [2016] reconstructs each image pixel as a set of RGB layers, so changing a palette color has a straightforward impact on the resulting image. Our recoloring result is similar to Tan et al.’s, with the difference being that we replace KM pigments in the extracted palette with other KM pigments (from Okumura [2005]) and re-render the image, creating different mixed colors in the style of real traditional media paints. Fig. 13a shows three examples. To enable a more direct comparison, we use our extracted palette RGB colors as the layer colors in Tan2016. In the cat painting, the KM mixing weight map for the blue pigment is sparse and therefore the recoloring effect is localized on the body of the cat. The weight map from Tan2016 has non-zero values in the background resulting in recoloring artifacts. For the rooster painting,



**Figure 11:** Adjusting the absolute mixing weight of a pigment without re-normalizing the weight sum creates variations that would be difficult to reproduce in RGB.

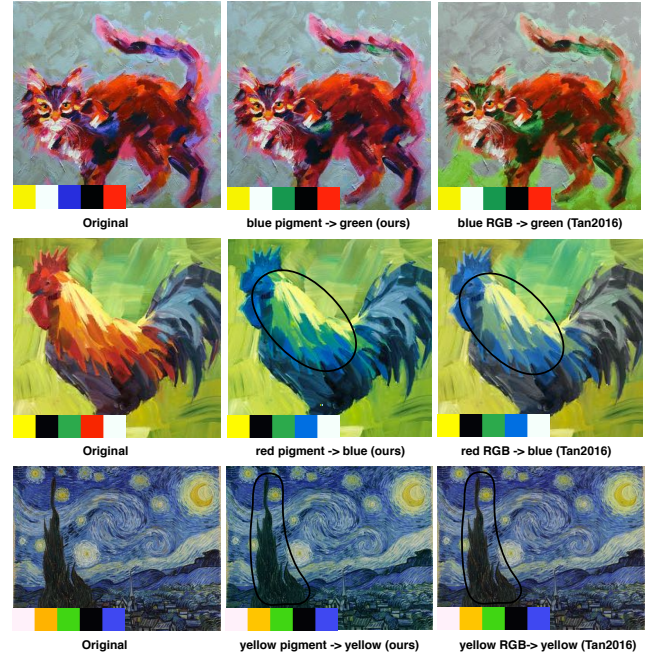


**(a)** Adjusting the absolute mixing weights of black and white pigments. The effects (middle two images) are different from adjusting the brightness level using photo manipulation software (rightmost image). Increasing the mixing weights of all layers (bottom left image) results in pigments reaching their respective massstones.

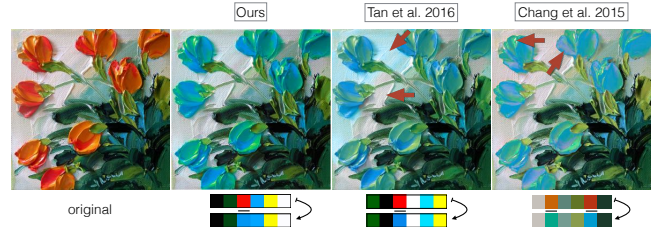


**(b)** Adjusting the scattering coefficients of the green pigment. Changing the scattering coefficients produces different effect from manipulating the mixing weights (rightmost image).

**Figure 12:** Tonal adjustments in pigment space.



**(a)** We use our palette's RGB colors for layers in Tan2016 for direct comparison. Top: blue is replaced by green. Middle: red is replaced by blue. Bottom: yellow is replaced with a different yellow.



**(b)** Each method extracts its own palette from the input image, so we attempt to mimic our result as closely as possible. Tan2016 suffers from lack of sparsity, while Chang2015 has surprising local colors (red arrows).

**Figure 13:** Recoloring comparisons.

using our KM model, more vibrant green is obtained from mixing yellow and blue in the circled region. For Starry Night, when swapping the extracted yellow pigment with a different yellow, the KM recoloring result reveals the green hue in the new yellow pigment, whereas the RGB recoloring result is similar to the original painting since the two yellow pigments have similar mass tones in RGB space. Fig. 13b shows a different recoloring comparison between Tan2016, Chang2015 and ours. Both Tan2016 and Chang2015 have color artifacts when using their own pipelines to recolor the painting to be similar to our result.

## 6.4 Cut, Copy, Paste

From a selection mask, we can use the pigment weight maps to do painterly cut, copy, and paste operations on images as well. For copy-paste, the user can specify a mask (using any mechanism) and the subset of pigments to copy. The selected region can then be pasted elsewhere as a new layer of paint on top of the image and re-composited. The paste operation can adjust paint properties simultaneously such as the thickness of the pasted layer, to achieve different compositing results, or can be added into the mixture model





**Figure 14:** Results of copy paste in pigment space. Each classical painting has been modified by selecting some set of pigments from a region of pixels, and adding them as a new layer on top elsewhere in the image. While the pasted regions are not identical to the copied regions (as they would be with standard RGB copy paste), they appear as if they were painted as part of the image.

as additional paint mixed into the painting layer, with relative scaling and renormalization. These options result in different painterly variations on standard image copy-pasting (Fig. 14 and Fig. 1).

The cut operation deletes the selected pixels’ pigments from the painting, for which inpainting fills the resulting hole (Fig. 1). We use a fast marching method [Telea 2004], though alternatives such as PatchMatch [Barnes et al. 2009] would also work, so long as they can operate on arbitrary numbers of image channels.

## 6.5 Palette Summarization

The first stage of our algorithm can also be seen as yet another method for extracting a small palette from an arbitrary image, not necessarily of paintings. Tan et al. [2016] and Chang et al. [2015] both present palette-extraction methods, as does Adobe’s Color CC app [2016]. We compare these results in Fig. 15a, where it is clear to see that Chang2015 and Kuler attempt to find “salient” or meaningful colors in some sense, whereas Tan2016 and our work focus on colors that reconstruct the images. We achieve similar results to Tan2016, but as we showed earlier our reconstructions are much lower error for the same number of colors, as we have more success with paint-like color mixtures such as green and cyan.

We can also use our palette extraction method to analyze collections of images, by amending our method to jointly reconstruct the pixels of multiple images. We use this approach to extract aggregate palettes from paintings of Van Gogh organized by year (Fig. 15b). Two results are clear from this analysis – first, that the range of colors Van Gogh painted with expanded over the 1880s, as we expanded from eight pigments to ten pigments to achieve good reconstruction errors, and second, that the vibrancy increased dramatically as well.

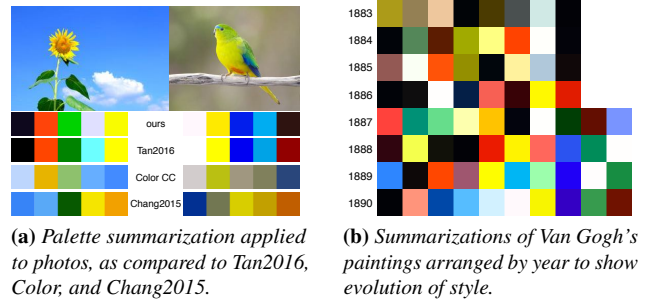


**Figure 15:** Examples of palette summarization.



**Figure 16:** Paint-aware edge detection and enhancement.

## 6.6 Edge Detection and Enhancement

Our weight maps can improve edge-based image analysis (Fig. 16). We apply an existing edge detection method [Isola et al. 2014] to each weight map separately and merge the per-pigment response as the per-pixel max. Paint edge images can be used to adapt standard image processing routines to be paint-aware. For example, we do edge enhancement by thickening pigments near boundaries according to the edge response, which can visually emphasize painted objects in a different way than RGB edge enhancement.

## 7 Conclusion

We demonstrate a method that can recover plausible physical pigments from only an RGB image of a painting, and then recover the mixing proportion of those pigments at each pixel. We are able to accurately reconstruct the RGB values of the image, and even closely match multispectral reflectance per-pixel as well, though the underlying pigment coefficients may differ. We use this decomposition to enable a number of image editing operations that occur in “pigment space,” which creates results in a style more consistent with natural media imagery rather than digital RGB edits.

In the future, we would like to extend our result to estimate pigment layers instead of just mixtures. We plan to use our decomposition to help extract brush stroke-level structure from images of paintings, to enable manipulation of the brush strokes in painting images. In general, we feel our strategy of interpreting deep structure from images to enable high-level edits will have applications in many other aspects of computer graphics.

## References

- ADOBE, 2016. Adobe Color CC. <https://color.adobe.com>.
- BARBER, C. B., DOBKIN, D. P., AND HUHDANPAA, H. 1996. The quickhull algorithm for convex hulls. *ACM Trans. Math. Softw.* 22, 4 (Dec.), 469–483.
- BARNES, C., SHECHTMAN, E., FINKELSTEIN, A., AND GOLDMAN, D. B. 2009. PatchMatch: A randomized correspondence

- algorithm for structural image editing. *ACM Trans. Graph.* 28, 3 (Aug.), 24:1–24:11.
- BARRON, J. T., AND POOLE, B. 2016. The fast bilateral solver. *ECCV*, 617–632.
- BAXTER, W. V., WENDT, J., AND LIN, M. C. 2004. IMPaSTo: A realistic, interactive model for paint. In *NPAR*, 45–56.
- BERNS, R. S., AND IMAI, F. H. 2002. The use of multi-channel visible spectrum imaging for pigment identification. In *ICOM-CC*, 217–222.
- BERNS, R., TAPLIN, L., AND NEZAMABADI, M. 2005. Spectral imaging using a commercial colour-filter array digital camera. In *ICOM-CC*, 743–750.
- BERNS, R. S., TAPLIN, L. A., IMAI, F. H., DAY, E. A., AND DAY, D. C. 2005. A comparison of small-aperture and image-based spectrophotometry of paintings. *Studies in Conservation* 50, 4, 253–266.
- BERNSTEIN, G. L., AND LI, W. 2015. Lillicon: Using transient widgets to create scale variations of icons. *ACM Trans. Graph.* 34, 4 (July), 144:1–144:11.
- BOLDRINI, B., KESSLER, W., REBNER, K., AND KESSLER, R. 2012. Hyperspectral imaging: a review of best practice, performance and pitfalls for inline and online applications. *Journal of Near Infrared Spectroscopy* 20, 5, 438–508.
- CHANG, H., FRIED, O., LIU, Y., DiVERDI, S., AND FINKELSTEIN, A. 2015. Palette-based photo recoloring. *ACM Trans. Graph.* 34, 4 (July).
- COSENTINO, A. 2014. Identification of pigments by multispectral imaging; a flowchart method. *Heritage Science* 2, 1, 8.
- CURTIS, C. J., ANDERSON, S. E., SEIMS, J. E., FLEISCHER, K. W., AND SALESIN, D. H. 1997. Computer-generated watercolor. In *SIGGRAPH*, 421–430.
- DUNCAN, D. R. 1940. The colour of pigment mixtures. *Proceedings of the Physical Society* 52, 3, 390.
- IBRAHIM, A., HORIUCHI, T., TOMINAGA, S., AND ELLA HASSANIEN, A. 2016. Spectral reflectance images and applications. In *Image Feature Detectors and Descriptors: Foundations and Applications*, A. I. Awad and M. Hassaballah, Eds. 227–254.
- ISOLA, P., ZORAN, D., KRISHNAN, D., AND ADELSON, E. H. 2014. Crisp boundary detection using pointwise mutual information. In *ECCV*, 799–814.
- KAUVAR, I., YANG, S. J., SHI, L., MCDOWALL, I., AND WETZSTEIN, G. 2015. Adaptive color display via perceptually-driven factored spectral projection. *ACM Trans. Graph.* 34, 6 (Oct.), 165:1–165:10.
- KUBELKA, P., AND MUNK, F. 1931. An article on optics of paint layers. *Zeitschrift für Technische Physik* 12, 593–601.
- KUBELKA, P. 1948. New contributions to the optics of intensely light-scattering materials. Part I. *Journal of the Optical Society of America* 38, 5, 448–448.
- KWOK, K., AND WEBSTER, G., 2016. Project Naptha: highlight, copy, and translate text from any image. <https://projectnaptha.com/>. Accessed: 2017-01-15.
- LIN, S., FISHER, M., DAI, A., AND HANRAHAN, P. 2017. Layer-Builder: Layer decomposition for interactive image and video color editing. 1–12. arXiv:1701.03754 [cs.GR].
- LU, J., DiVERDI, S., CHEN, W. A., BARNES, C., AND FINKELSTEIN, A. 2014. RealPigment: Paint compositing by example. In *NPAR*, 21–30.
- OHTA, N., AND ROBERTSON, A. R. 2006. *CIE Standard Colorimetric System*. John Wiley & Sons, Ltd, 63–114.
- OKUMURA, Y. 2005. *Developing a spectral and colorimetric database of artist paint materials*. Master’s thesis, Rochester Institute of Technology.
- PARK, J.-I., LEE, M.-H., GROSSBERG, M. D., AND NAYAR, S. K. 2007. Multispectral imaging using multiplexed illumination. In *ICCV*, 1–8.
- PARMAR, M., LANSEL, S., AND FARRELL, J. 2012. An LED-based lighting system for acquiring multispectral scenes. In *Digital Photography VIII*.
- PELAGOTTI, A., MASTIO, A. D., ROSA, A. D., AND PIVA, A. 2008. Multispectral imaging of paintings. *IEEE Signal Processing Magazine* 25, 4 (July), 27–36.
- ROTHER, C., KOLMOGOROV, V., AND BLAKE, A. 2004. “GrabCut” — interactive foreground extraction using iterated graph cuts. *ACM Trans. Graph.* 23, 3, 309–314.
- TAN, J., DVOROŽŇÁK, M., SÝKORA, D., AND GINGOLD, Y. 2015. Decomposing time-lapse paintings into layers. *ACM Trans. Graph.* 34, 4 (July), 61:1–61:10.
- TAN, J., LIEN, J.-M., AND GINGOLD, Y. 2016. Decomposing images into layers via RGB-space geometry. *ACM Trans. Graph.* 36, 1 (Nov.), 7:1–7:14.
- TELEA, A. 2004. An image inpainting technique based on the fast marching method. *JGT* 9, 1, 23–34.
- XU, S., TAN, H., JIAO, X., LAU, F. C., AND PAN, Y. 2007. A generic pigment model for digital painting. *Computer Graphics Forum*.
- ZHAO, Y., BERNS, R. S., OKUMURA, Y., AND TAPLIN, L. A. 2005. Improvement of spectral imaging by pigment mapping. In *Color and Imaging Conference*, 40–45.
- ZHAO, Y., BERNS, R. S., TAPLIN, L. A., AND CODDINGTON, J. 2008. An investigation of multispectral imaging for the mapping of pigments in paintings. In *Electronic Imaging*.
- ZHU, C., BYRD, R. H., LU, P., AND NOCEDAL, J. 1997. Algorithm 778: L-BFGS-B: Fortran subroutines for large-scale bound-constrained optimization. *ACM Trans. Math. Softw.* 23, 4 (Dec.), 550–560.